JOURNAL OF CATALYSIS **167,** 364–371 (1997)
ARTICLE NO. CA971578

XAFS Characterization of Pt–Mo Bimetallic Catalysts for CO Hydrogenation

Sun Hee Choi and Jae Sung Lee[1]

Department of Chemical Engineering and School of Environmental Engineering, Pohang University of Science and Technology (POSTECH) and Research Institute of Industrial Science and Technology (RIST), San 31 Hyoja-dong, Pohang 790-784, Republic of Korea

Received June 27, 1996; revised December 19, 1996; accepted December 20, 1996

Molybdenum–platinum bimetallic catalysts supported on alumina exhibited high activities in CO hydrogenation than supported monometallic catalysts of Mo or Pt. The structure of Mo–Pt bimetallic catalysts, which were prepared by incipient wetness impregnation of γ-alumina with the variation of the order of Mo and Pt addition, was studied by XAFS and CO chemisorption. Since molybdenum contains overlapping contribution of the first and the second shells, EXAFS of these two shells and the first shell of platinum was analyzed for the bimetallic catalysts. EXAFS showed equivocally the formation of bimetallic bonds between Mo and Pt for all bimetallic catalysts. For all bimetallic catalysts, molybdenum seemed to segregate to the surface irrespective of the sequence of the impregnation. Strong interaction of Mo atoms with the support was also identified with EXAFS and XANES for both monometallic Mo catalysts and bimetallic catalysts. Regarding the activities of CO hydrogenation, it was concluded that reduced Mo sites were responsible for the high activity and that Pt helped Mo sites become more reduced.

INTRODUCTION

Bimetallic catalysts which consist of Mo and Pt have shown high activity in hydrogenolysis of alkanes (1–3) and dehydrogenation of cyclohexane (4), while comparable activity was not observed for the monometallic catalysts. In hydrogenolysis of ethane, Yermakov *et al*. (1) suggested that the higher activity of the bimetallic catalyst was due to the change in electronic properties of the platinum caused by its interaction with the molybdenum on a support. Tri *et al*. (2, 3) concluded that the addition of Mo made initially electron deficient Pt particles be similar to bulk Pt, but that the enhanced activity was due to complementary role of Pt and Mo on adsorption of reactants. Leclercq *et al*. (4) approached the problem with a more detailed adsorption measurement and XPS study. By measuring the degree of oxidation of molybdenum, they related the higher activity to molybdenum, modified by addition of Pt in the bimetallic catalyst. From these studies, it is clear that the each metal component has a specific role on the effectiveness of the bimetallic catalyst. Thus, it is expected that understanding of the structure of Pt–Mo bimetallic catalysts would help clarify the role of each metal.

The X-ray absorption fine structure (XAFS) has been of great use in studying the structure of supported catalysts, and of multicomponent catalysts in particular. The extended X-ray absorption fine structure (EXAFS), which is one area of XAFS, contains information on local atomic arrangement about each individual type of absorber atom as described in theoretical formula based on the single contribution to XAFS (5). On the other hand, X-ray absorption near-edge structure (XANES), which represents electronic transitions from inner electronic levels to outer unoccupied levels caused by X-ray absorption, reveals information on the electronic structure of condensed matter, including differences in chemical environment, the oxidation state in complex, and so on (6, 7). Since this short-range order characteristic of XAFS avoids the limitations of some other physical and chemical probes, many investigators have applied XAFS to obtain information on supported catalysts since the seventies. Sinfelt extensively studied bimetallic catalysts such as ruthenium–copper, osmium–copper, platinum–iridium, and platinum–ruthenium by means of EXAFS as a structural tool (8). For Pt–Mo catalyst, Samant *et al*. have employed EXAFS and anomalous wide-angle X-ray scattering (AWAXS) to investigate the structure of Pt–Mo bimetallic clusters which were prepared by the deposition of $Mo(CO)_6$ vapor on preformed Pt/Y–zeolites (9, 10). It was concluded that Pt in the bimetal clusters had an atomic structure similar to that of bulk Pt and was surrounded by epitaxially deposited Mo. Because of the epitaxy, Mo–Mo and Mo–Pt distances in the bimetallic clusters were found to be identical to that of Pt–Pt.

The unique structural features of Mo–Pt/Y-zeolite reported by Samant *et al*. (9, 10) may have originated from the unconventional preparation method, of chemical vapor deposition on preformed Pt clusters. Hence, in the present work, we have studied the Mo–Pt bimetallic catalysts

[1] To whom correspondence should be addressed. Fax: 82-562-279-5799.

0021-9517/97 $25.00

prepared by the conventional method of impregnation using aqueous solutions of inorganic metal salts. The sequence of metal addition and the temperature of reduction were varied and the catalysts were characterized mainly by XAFS. The activity in CO hydrogenation of bimetallic catalysts was compared with that of monometallic Pt or Mo catalysts.

EXPERIMENTAL

Sample Preparation

The materials for the catalyst preparation were $(NH_4)_6Mo_7O_{24}\cdot 4H_2O$ (Aldrich) and $H_2PtCl_6\cdot 6H_2O$ (Strem Chemicals, 38.85% Pt) as the metal precursors. The support for the metals was γ-Al_2O_3 (Alfa, 99%, 3.2 mm pellets) crushed into the powder of 60–100 mesh (BET area, 202 $m^2\ g^{-1}$; porosity which is defined as pore volume of a particle divided by the total volume of the particle, 0.43). For the monometallic catalysts, a solution of a metal salt was added to γ-Al_2O_3 by incipient wetness impregnation in an amount that would give 5 wt% loading of the metal. The catalysts were then dried for 12 h at 380 K and calcined for 12 h at 770 K. The three kinds of bimetallic catalysts denoted as Mo–Pt/γ-Al_2O_3, Pt–Mo/γ-Al_2O_3, and Mo + Pt/γ-Al_2O_3 were prepared with variation of the order of addition of molybdenum and platinum. In the case of Mo–Pt/γ-Al_2O_3, Mo/γ-Al_2O_3 was prepared first and following the drying and calcination steps, the solution of platinum salt was added by incipient impregnation with the 1 : 1 atomic ratio of molybdenum to platinum keeping the Pt loading at 5 wt%. The resulting bimetallic catalysts were then treated by the same drying and calcination procedures as in the case of monometallic catalysts. Similarly, the Pt–Mo/γ-Al_2O_3 catalysts were prepared by the addition of the solution of molybdenum salt to calcined Pt/γ-Al_2O_3 and treated under the same drying and calcination conditions. Mo + Pt/γ-Al_2O_3 catalysts were prepared by coimpregnation.

XAFS Measurements and Data Analysis

For the XAFS measurements, the prepared catalysts were pelletized into a appropriate thickness that would give the absorbance of ca. 1 at the edge energy. Thus, the optimum thickness depended on the kind of metal and X-ray absorption edge. The sample disc was placed in a cell designed for *in situ* experiments (11). The catalyst discs in the U-tube reactor with the attached spectroscopic cell were reduced in flowing H_2 at one of three temperatures: either 773, 973, or 1073 K, for 2 h. After the sample treatment, the reactor was inverted for the sample to be sent into the bottom part of the cell and located between two Kapton windows where X-ray would pass through during the measurement. Then, the cell was disconnected from the reactor by a flame, with the sample still under the same gas atmosphere as for the reduction.

XAFS measurements for the samples in the sealed spectroscopic cell were performed on BL10B of Photon Factory (electron energy in the storage ring, 2.5 GeV; maximum current, 360 mA) in National Laboratory for High Energy Physics (KEK) in Japan. At room temperature, the spectra were taken for K-edges of Mo with the detector gases of Ar(100%) for the incident beam and N_2(85%) + Ar(15%) for the transmitted beam, and L_{III}-edges of Pt with detector gases of Ar(100%) and N_2(75%) + Ar(15%), respectively.

The obtained XAFS data were analyzed by the R-space method with UWXAFS 3.0 package and FEFF 6 code with the license from University of Washington (5). The initial data, which had been converted to the proper format for UWXAFS program, were first subject to preedge subtraction so as to remove the effects due to absorption by another edge or by other components. The preedge region was fitted with a polynomial spline and then extrapolated beyond the edge and subtracted from total absorption to give the elemental absorption $\mu(E)$. To get EXAFS function $\chi(k)$, which is defined by $\chi(E) = [\mu(E) - \mu_0(E)]/\mu_0(E)$, the unknown $\mu_0(E)$ was approximated by a smooth curve $\mu_{\text{spline}}(E)$. Then, the postedge background removed $\Delta\mu(E) = \mu(E) - \mu_0(E)$ was normalized with respect to $\mu_0(E)$. The EXAFS function $\chi(k)$ of momentum space was converted to real space, i.e., R-space by the Fourier transformation to obtain the radial structural function (RSF) for each sample (12, 13). The range Δk for the Fourier transformation was 2.30–14.45 ($Å^{-1}$) for Pt L_{III}-edges and 2.20–12.80 ($Å^{-1}$) for Mo K-edges, with Hanning window sills and window sill width of $dk = 1.0$. The standards for fitting were theoretically synthesized with the FEFF code and the data were fitted in the R-space. A single adjustable parameter in XAFS analysis, amplitude reduction factor (S_0^2) was taken to be 0.95 for Pt and 0.83 for Mo, which were found by fitting of experimental RSFs of metal foils with theoretical ones.

CO Chemisorption

About 0.25 g of catalyst was loaded into a cell for chemisorption, reduced in flowing H_2, and then purged with He at temperature slightly higher than the reduction temperature to remove all hydrogen adsorbed during the reduction. The cell was moved to a conventional volumetric adsorption apparatus (Micrometrics Model AccuSorb 2100E) without exposure of the sample to air. Before measuring CO uptake, the sample was evacuated for 2 h at 423 K to a pressure less than 10^{-3} Pa and cooled under vacuum to room temperature. The first CO isotherm was taken at increasing CO pressures and following evacuation at room temperature for 1 h, the second isotherm was taken in a similar way. The amount of irreversible CO uptake was

obtained from the difference between the two isotherms which were extrapolated to zero pressure.

CO Hydrogenation

Before the reaction, the catalysts were treated under the same pretreatment conditions as those for XAFS measurements. CO hydrogenation was carried out in a flow reactor at 573 K and atmospheric pressure with H_2/CO feed ratio of 3.0. The reaction products were analyzed using a gas chromatograph (Perkin Elmer, Model 8500) equipped with a thermal conductivity detector and a 1.5 m long, 3.2 mm diameter column packed with Porapak-Q materials by which CO, CO_2, and CH_4 were analyzed, and a flame ionization detector and a 3.0 m long, 3.2 mm diameter column packed with Porapak-Q materials by which hydrocarbons including CH_4 were analyzed.

RESULTS

CO Chemisorption and CO Hydrogenation

The result of CO Chemisorption for (Mo,Pt)/γ-Al_2O_3 is given in Table 1. The CO uptakes of Pt/γ-Al_2O_3 are generally large. However, CO uptakes of Mo/γ-Al_2O_3 are very small on three reduction temperatures, indicating the difficulty involved in the reduction of Mo/γ-Al_2O_3. For the bimetallic catalysts, CO uptakes stand between those of Pt/γ-Al_2O_3 and Mo/γ-Al_2O_3 and decrease slightly as the reduction temperature increases.

Meanwhile, the activities for CO hydrogenation of the catalysts reduced at 773 K (A), 973 K (B), and 1173 K (C) are given in Fig. 1. In almost all cases, the CO activities are very large for bimetallic catalysts compared with those for monometallic catalysts. The activities are expressed in terms of apparent turnover frequencies (TOF) defined as numbers of CO molecule converted to products per second per site measured by CO chemisorption at room temperature. As the reduction temperature of the catalyst increases, increase in activity was evident. Furthermore, there was a rapid decrease in catalytic activity as the reaction proceeded for the bimetallic catalysts reduced at 1173 K.

TABLE 1

CO Uptakes of (Mo,Pt)/γ-Al_2O_3 Catalysts at Room Temperature

Catalysts	CO uptake/μmol (g-metal)$^{-1}$		
	773 K[a]	973 K[a]	1173 K[a]
Pt/γ-Al_2O_3	916	236	320
Pt–Mo/γ-Al_2O_3	420	387	321
Mo + Pt/γ-Al_2O_3	174	205	201
Mo–Pt/γ-Al_2O_3	284	165	134
Mo/γ-Al_2O_3	70	74	22

[a] Reduction temperature.

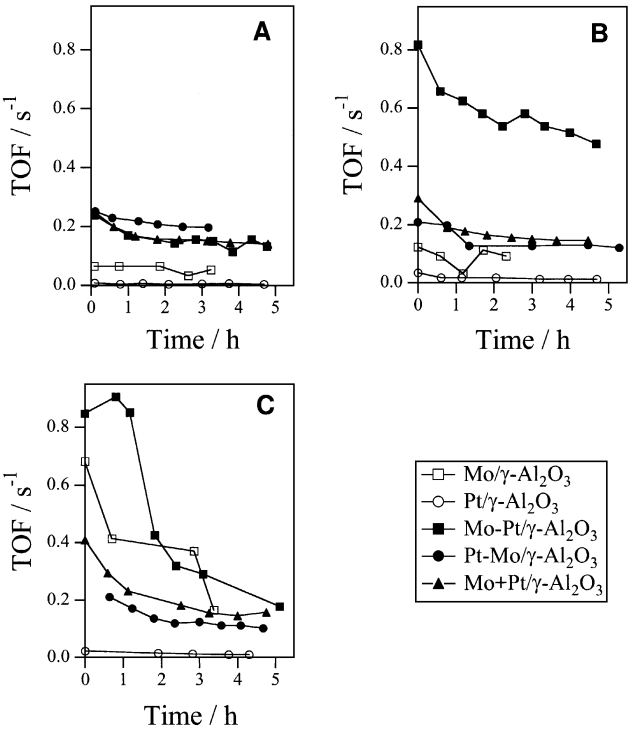

FIG. 1. Change with time on stream in turnover frequencies (TOF) of CO conversion during CO hydrogenation over monometallic and bimetallic catalysts: (A) after reduction at 773 K; (B) after reduction at 973 K; and (C) after reduction at 1173 K. Reaction conditions: atmospheric pressure, H_2/CO = 3; total flow rate, 37.3 cm^3/min; catalyst charge, 0.2 g.

EXAFS and XANES of Monometallic Catalysts

The weighted EXAFS function $k^3\chi(k)$ and RSF for Pt/γ-Al_2O_3 are shown in Fig. 2. The peak position and the shape in RSF are nearly same as those of Pt foil. The coordination numbers of monometallic catalysts are all similar and substantially smaller than that of bulk platinum metal as shown in Table 2. The Pt–Pt interatomic distance is consistently smaller than that of bulk Pt. The Debye–Waller factors for supported catalysts, which are an index of the disorder both in structural and thermal aspects, are larger than that of bulk Pt.

The EXAFS analysis of Mo/γ-Al_2O_3, shown in Fig. 3, is more complicated due to the substantial overlap of two peaks located at radial distances between 2 and 3 Å that resulted from the backscattering by the first and the second nearest neighbor molybdenum atoms. The actual distances corresponding to these peaks are 2.725 and 3.149 Å. This was also confirmed by a theoretical calculation with FEFF6. The calculation with only the first nearest neighbor atoms gave a peak at the same position as for the first peak in Fig. 3B between 2 and 3 Å and the calculation with only the second nearest neighbors gave a peak at the same position as that for the second peak. Samant *et al.* also treated this problem in their study by using a two-shell fit of $\chi(k)$ for the Mo foil (10). Accordingly, we used two paths as the

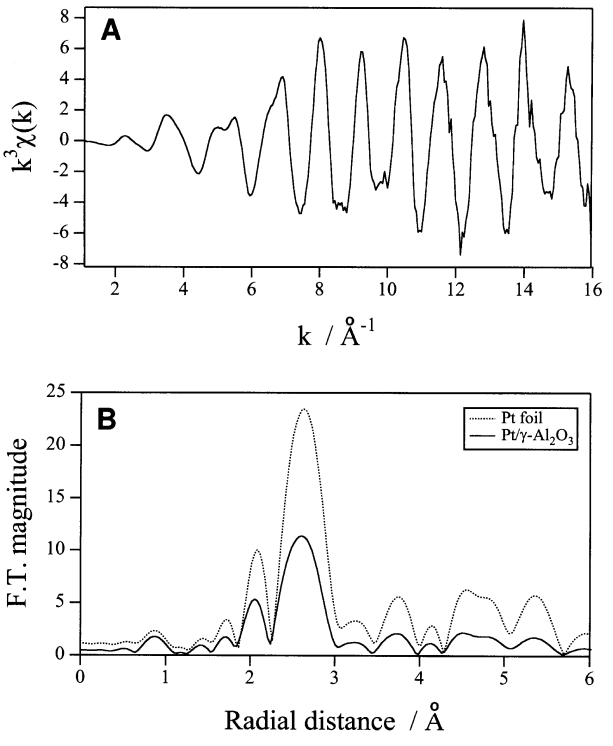

FIG. 2. EXAFS of Pt/γ-Al_2O_3 reduced at 973 K. (A) EXAFS function; (B) RSF.

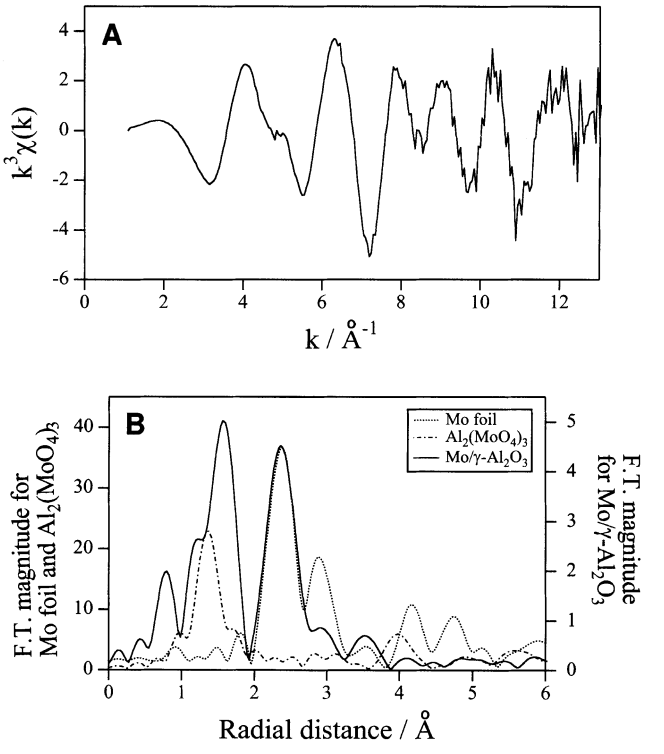

FIG. 3. EXAFS of Mo/γ-Al_2O_3 reduced at 973 K. (A) EXAFS function; (B) RSF. The RSF of $Al_2(MoO_4)_3$ was calculated by using FEFF 6 code.

standard for fitting and carried out a two-shell fit for the RSFs of all Mo/γ-Al_2O_3 catalysts.

The results of two-shell fittings of Mo/γ-Al_2O_3 are also given in Table 2. A peculiar result is that coordination numbers of Mo–Mo are very small, even considering the fact that Mo might be well dispersed on the support. This is consistent with the qualitative result that the magnitude of the Mo–Mo peak in Mo/γ-Al_2O_3 is just one-seventh of that in Mo foil (Fig. 3).

As shown in Fig. 4, the XANES of Pt L_{III}-edge of Pt/γ-Al_2O_3 does not show any difference from that of Pt foil, whereas there exists significant difference between the XANES of Mo foil and that of Mo/γ-Al_2O_3.

TABLE 2

EXAFS Curve Fitting Results of Metal Foil and Pt/γ-Al_2O_3 and Mo/γ-Al_2O_3 Catalysts Reduced at Different Temperatures

Reduction temperature (K)	N(Pt–Pt)[a]	R(Pt–Pt) (Å)[b]	$\sigma^2 \times 10^3$ (Å^2)[c]
Pt foil	12.0	2.775	4.4
773	7.4	2.75	6.0
973	7.8	2.74	6.2
1173	7.5	2.73	6.4

	N(Mo–1Mo)[d]	N(Mo–2Mo)[e]	R(Mo–1Mo)[f] (Å)	$\sigma^2 \times 10^3$ (Å^2)[g]
Mo foil	8.0	6.0	2.725	3.3
973	2.5	0.2	2.67	4.5
1173	1.7	1.1	2.64	4.6

[a] N, coordination number.
[b] R, distance between atoms.
[c] σ^2, Debye–Waller factor.
[d] N between absorber Mo and the first nearest backscatter Mo.
[e] N between absorber Mo and the second nearest backscatter Mo.
[f] R between absorber Mo and the first nearest backscatter Mo.
[g] σ^2 between absorber Mo and the first nearest backscatter Mo.

EXAFS and XANES of Bimetallic Catalysts

Owing to the contribution from the second shell atoms in Mo, we considered the following EXAFS functions for the bimetallic catalysts,

$$[\chi(k)]_{Pt} = [\chi'(k)]^{Pt}_{Pt} + [\chi'(k)]^{1Mo}_{Pt} + [\chi'(k)]^{2Mo}_{Pt}$$

$$[\chi(k)]_{Mo} = [\chi'(k)]^{1Mo}_{Mo} + [\chi'(k)]^{2Mo}_{Mo} + [\chi'(k)]^{Pt}_{1Mo} + [\chi'(k)]^{Pt}_{2Mo},$$

where the subscript outside the square bracket identifies the absorber atom, while the superscript identifies the backscattering atom. The numbers 1 and 2 represent the first and the second shell atoms, respectively. Thus the fittings over all bimetallic samples were carried out first for Pt L_{III}-edges using three standards, then, based on the criterion for fitting of bimetallic catalysts that the distance on absorber–backscatterer pair on either side of edge should be the same (8), the second fitting was performed for Mo K-edges with

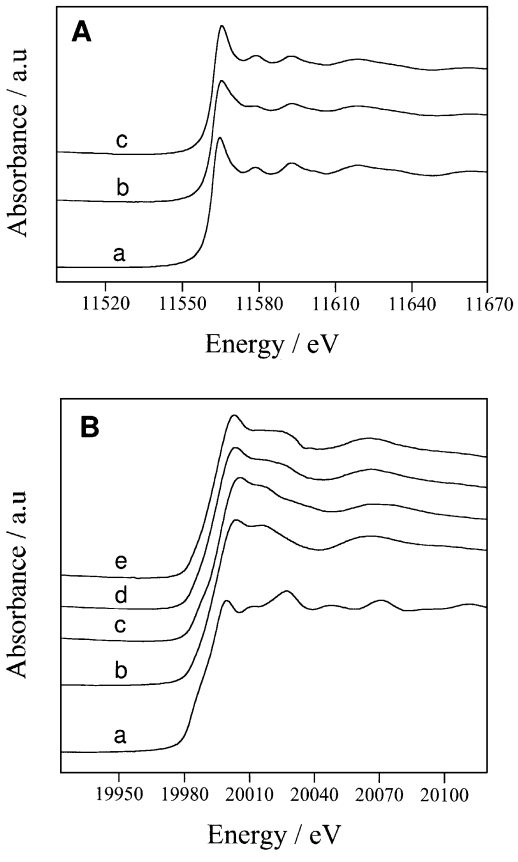

FIG. 4. (A) XANES of Pt L_{III}-edge. (a) Pt foil; (b) Pt/γ-Al_2O_3 reduced at 973 K; (c) Pt–Mo/γ-Al_2O_3 reduced at 973 K. (B) XANES of Mo K-edge. (a) Mo foil; (b) Mo/γ-Al_2O_3 reduced at 973 K; (c) Pt–Mo/γ-Al_2O_3 catalysts reduced at 773 K; (d) the same reduced at 973 K; (e) the same reduced at 1173 K.

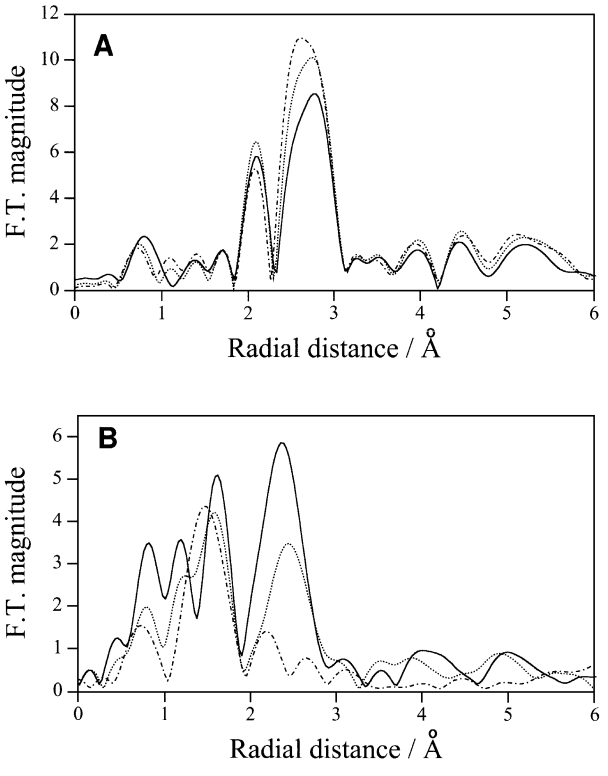

FIG. 5. (A) RSFs from Pt L_{III}-edge of Pt–Mo/γ-Al_2O_3. (B) RSFs from Mo K-edge of Pt–Mo/γ-Al_2O_3. The catalysts were reduced at 773 K (– -), 973 K (· · ·), and 1173 K (—).

four standards. Taking into account the fact that EXAFS spectra contain about 12 structural parameters, it becomes less meaningful to get all the parameters for each standard. Thus we did not considered the Debye–Waller factors for the standards containing the second shell Mo atom whose effect was found to be insignificant.

The RSFs of Pt–Mo/γ-Al_2O_3 are given in Fig. 5 for Pt L_{III}-edge (A) and for Mo K-edge (B), respectively. There are no extra metal–metal peaks which would represent the alloy formation between Pt and Mo in either case. Yet, this is an expected result because of the similarity between interatomic distances of Pt–Pt and Mo–Mo. However, the asymmetric peak shape in the RSF for Pt L_{III}-edge strongly suggests the presence of a metal–metal distance other than the Pt–Pt distance.

The curve fitting results of Pt–Mo/γ-Al_2O_3 are given in Table 3. With increasing treatment temperatures, the distance between molybdenum atoms decreases, while that between platinum and molybdenum increases slightly. But, the distance between platinum atoms does not show any variation with the treatment temperature. The coordination numbers of Pt–Pt in Pt–Mo/γ-Al_2O_3 are about 7, and those of Mo–Pt and Pt–Mo increase with increasing treatment temperature, implying increased formation of an alloy. However, the coordination number of Mo–Mo is very small, like that of Mo–Mo in Mo/γ-Al_2O_3, and shows a

TABLE 3

EXAFS Curve Fitting Results of Pt–Mo/γ-Al_2O_3 Catalysts Reduced at Different Temperatures[a]

Reduction temperature (K)	N(Pt–Pt)	N(Pt–Mo)	N(Mo–Pt)	N(Mo–Mo)	R(Pt–Pt)	R(Pt–1Mo)	R(Mo–1Mo)	$\sigma^2 \times 10^3$(Pt–Pt)	$\sigma^2 \times 10^3$(Pt–1Mo)
773	7.3	0.3	0.8	0.3	2.77	2.65	2.74	4.2	14.6
973	7.9	1.0	2.8	1.2	2.76	2.72	2.74	4.5	9.9
1173	7.3	1.2	2.4	2.4	2.77	2.72	2.68	5.7	9.2

[a] Distance (R) in Å and Debye–Waller factor (σ^2) in Å^2.

TABLE 4

EXAFS Curve Fitting Results of Mo + Pt/γ-Al_2O_3 and Mo–Pt/γ-Al_2O_3 Catalysts Reduced at Different Temperatures[a]

Reduction temperature (K)	N(Pt–Pt)	N(Pt–Mo)	N(Mo–Pt)	N(Mo–Mo)	R(Pt–Pt)	R(Pt–1Mo)	R(Mo–1Mo)
			Mo + Pt/γ-Al_2O_3				
773	7.7	1.6	0.6	0.7	2.76	2.83	2.67
973	8.0	3.3	2.3	2.3	2.76	2.77	2.76
1173	7.0	2.2	2.4	3.3	2.75	2.75	2.74
			Mo–Pt/γ-Al_2O_3				
773	6.7	0.4	0.8	0.4	2.74	2.69	2.76
1173	4.9	1.2	2.4	2.6	2.69	2.71	2.69

[a] Distances (R) in Å.

rapid increase with increasing reduction temperatures. In Pt–Mo/γ-Al_2O_3 reduced at 773 K, the existence of Mo–Mo distances is barely identified with a very small magnitude of the peak, in Fig. 5B.

The results of curve fitting of Mo–Pt/γ-Al_2O_3 and Mo + Pt/γ-Al_2O_3 are also given in Table 4. In two systems, for each absorber–backscatterer pair, the coordination numbers are nearly the same as those in Pt–Mo/γ-Al_2O_3. Only the coordination number of Pt–Pt in Mo–Pt/γ-Al_2O_3 is a little smaller than those found in other samples.

As far as XANES of Pt L_{III}-edge is concerned, there is no difference in shape among Pt/γ-Al_2O_3, Pt–Mo/γ-Al_2O_3, and Pt foil, as shown in Fig. 4A. Nevertheless, white line areas of Pt L_{III}-edge for bimetallic catalysts, which are known to be proportional to the number of d-band holes (7), are smaller than those of Pt/γ-Al_2O_3 catalysts and similar to that of Pt foil (Table 5). XANES of Mo K-edge for Mo–Pt/γ-Al_2O_3 shown in Fig. 4B has significantly different shapes from that of Mo foil, and is very similar to that of Mo/γ-Al_2O_3 reduced at 773 K. As the reduction temperature increases, XANES of Pt L_{III}-edge for Pt–Mo/γ-Al_2O_3 does not show any change, but that of Mo K-edge shows a significant change that makes the spectra look more like the Mo foil spectrum.

TABLE 5

White Line Area of Pt L_{III}-edge in (Mo,Pt)/γ-Al_2O_3 Catalysts Reduced at Different Temperatures

Catalyst		Area (eV cm^{-1})
Pt foil		9.70
Pt/γ-Al_2O_3	773 K	9.89
	973 K	9.90
	1173 K	9.88
Mo–Pt/γ-Al_2O_3	773 K	9.78
	1173 K	9.79
Pt–Mo/γ-Al_2O_3	773 K	9.69
	973 K	9.82
	1173 K	9.72
Mo + Pt/γ-Al_2O_3	773 K	9.71
	973 K	9.71
	1173 K	9.81

DISCUSSION

The coordination number of Pt–Pt in Pt/γ-Al_2O_3, which is smaller than that in Pt foil, indicates that platinum is well dispersed over the γ-Al_2O_3 support. Also, a larger Debye–Waller factor suggests that the supported platinum particles have more disordered structure compared to bulk Pt. The difference in Pt–Pt distance is small, but consistently shorter for supported samples. As shown in Table 5, the supported Pt shows increased white line area of Pt L_{III}-edge relative to Pt foil, indicating an electron deficient state in Pt/γ-Al_2O_3. The addition of Mo reduces the white line areas of Pt toward the values of Pt foil. The contraction of Pt–Pt distance and increased white line areas for supported Pt catalysts relative to bulk Pt are often observed (14, 15) and have been attributed to the small size of metal clusters (16). The conversion of the state of Pt in Pt/γ-Al_2O_3 into a state closer to that of bulk Pt by the addition of Mo may be taken as evidence for an electronic interaction between two metals.

Unlike the RSF of Pt/γ-Al_2O_3, the RSF of Mo/γ-Al_2O_3 shows unusual peaks in the distances of 1–2 Å, indicating the existence of light backscatterer atoms. These peaks are not originated from the presence of molybdenum oxides in the samples, because RSF and XANES of MoO_2 and MoO_3 are markedly different from that of Mo/γ-Al_2O_3. The other possibility is the interaction between Mo and the support γ-Al_2O_3. If this is the case, an intermetallide species such as $Al_2(MoO_4)_3$ may be formed during the calcination and/or reduction process. The theoretical RSF of $Al_2(MoO_4)_3$, synthesized with the theoretical XAFS code FEFF 6, is shown in Fig. 3B. The position of the major peaks does not correspond exactly to those of the peaks observed for Mo/γ-Al_2O_3. Yet, the closeness in positions of these peaks suggests the presence of similar intermetallic species in Mo/γ-Al_2O_3. After all, it is not expected that the species would have the stoichiometry and structure as well defined as theoretical $Al_2(MoO_4)_3$.

Such a strong interaction is also reflected in XANES of Mo/γ-Al_2O_3. The marked difference between Mo foil and Mo/γ-Al_2O_3 in peak shape represents the different states of molybdenum in catalyst and Mo foil. The shape of XANES observed for Mo/γ-Al_2O_3 was usually observed when molybdenum forms a compound (17–19). Incomplete reduction of molybdenum oxide does not appear to be the main cause of the XANES feature, because it would have shifted the edge position to a higher energy. Therefore, a strong interaction between molybdenum and the support appears responsible.

The coordination numbers for Mo/γ-Al_2O_3 are too small even considering the possibility of small particle sizes. Their shape is probably not sphere but like a "raft." It is well known that MoO_3 forms two-dimensional islands of one to several atoms thick on alumina (20). This morphology of the precursor may be maintained to some degree in reduced catalysts.

An interesting observation for the bimetallic catalysts is that the presence of the Pt–Mo pair is indicated in RSF of Pt EXAFS by the asymmetric shape of the largest peak before performing curve fitting. Unlike the result of Samant *et al.* (9, 10), the Pt–Mo distance is not same as the Pt–Pt distance. Thus, the asymmetric shape of peaks in RSFs in Fig. 5 suggests the presence of Pt–Mo scattering at a shorter distance in addition to usual Pt–Pt scattering. The results of curve fitting of Pt–Mo/γ-Al_2O_3 summarized in Table 3 confirm this observation. The result is not consistent with that reported by Samant *et al.* who observed a single peak in RSF and same distance for Pt–Pt, Pt–Mo, and Mo–Mo for Pt–Mo/Y-zeolite catalysts prepared by the deposition of $Mo(CO)_6$ vapor on Pt/Y-zeolite. They concluded that Mo was deposited epitaxially on Pt so that the Mo–Mo and Pt–Mo distances were identical to the Pt–Pt distance. It is not clear if the difference stems from the different preparation methods or from the improved resolution of data in the present study. In any case, the differences in Pt–Pt, Pt–Mo, and Mo–Mo distances are small (less than 0.12 Å) and Pt–Pt and Mo–Mo distances are almost the same for Pt–Mo/γ-Al_2O_3 catalysts reduced at 773 and 973 K.

From the relative magnitudes of coordination numbers of four absorber–scatterer pairs, the Pt–Mo/γ-Al_2O_3 can be described as alloy clusters where platinum atoms are surrounded by molybdenum. Thus, the Mo–Mo coordination number becomes smaller than Pt–Pt because Mo is located at the outer surface region, while Pt resides near the core of the cluster. Furthermore, the Mo–Mo distance is elongated to accommodate itself to the underlying Pt lattice. Hence, except for some minor details, the overall structure of Pt–Mo cluster described by Samant *et al.* (9, 10) is similar to what is observed in the present work despite of the widely different preparation methods.

An interesting observation was made when the Mo–Pt/γ-Al_2O_3 catalysts reduced at 973 K was exposed to air before

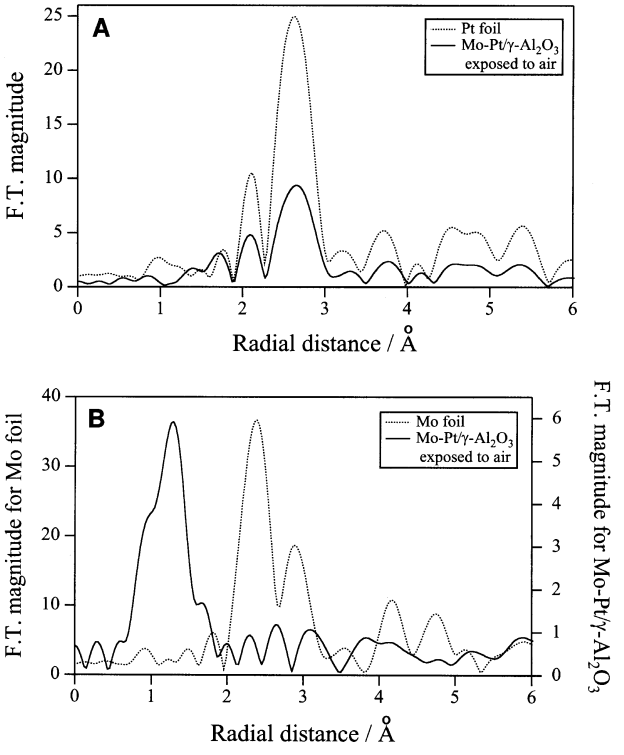

FIG. 6. (A) RSFs from Pt L_{III}-edge of air-exposed Pt–Mo/γ-Al_2O_3. (B) RSFs from Mo K-edge of air-exposed Pt–Mo/γ-Al_2O_3.

XAFS measurement. As shown in Fig. 6, the RSF for the Pt L_{III}-edge does not change compared with that for unexposed samples. In contrast, new peaks appears below 2 Å in the RSF from the Mo K-edge, which could be assigned to the formation of molybdenum oxides. This is an indication that the molybdenum surrounds platinum core in the bimetallic cluster.

The coordination numbers of Mo–Pt/γ-Al_2O_3 and Mo + Pt/γ-Al_2O_3 were similar to those of Pt–Mo/γ-Al_2O_3. Consequently, the overall structures of Mo–Pt/γ-Al_2O_3 and Mo + Pt/γ-Al_2O_3 are not greatly different from that of Pt–Mo/γ-Al_2O_3. Thus, it is concluded that structure of (Mo,Pt)/γ-Al_2O_3 bimetallic catalysts is not significantly affected by the sequence of impregnation of each metal. The result is a rather unexpected one because a stable structure of the initially added metal oxide would have been formed during the calcination step before the second metal was added. The observation is understood if at least one component is highly mobile during the final calcination or reduction steps. MoO_3 is probably the mobile species which could even be volatile at the calcination temperature of 770 K.

The structural feature of Mo–Pt/Al_2O_3 discussed so far has many things in common with that of Co–Pt/Al_2O_3 studied by Guczi and co-workers (21–23). A structural model based on the results of X-ray photoelectron spectroscopy, temperature-programmed reduction, and chemisorption of CO and H_2 suggested the presence of highly dispersed

platinum covered by metallic cobalt and a PtCo interphase. In addition, the presence of hardly reducible cobalt oxide layer was suggested. In the present study, no evidence has been found for the formation of a molybdenum oxide although molydenum oxides are known to be more difficult to be reduced than cobalt oxides (24). The much higher reduction temperatures employed in the present study (773–1173 K) compared to those of their work (570–720 K) may be responsible for the difference.

All bimetallic catalysts showed higher CO conversions and, in most cases, higher TOF values than monometallic catalysts for CO hydrogenation. The low activity of $Pt/\gamma\text{-}Al_2O_3$ is due to the intrinsic reactivity of the metal which is fully reduced as indicated by a large amount of CO chemisorption and XAFS results. Platinum is a known poor catalyst for CO hydrogenation with turnover frequencies (rate of CO conversion per site per unit time) about two orders of magnitude smaller than that of Ru at 548 K (25). In contrast, the low activity of Mo/Al_2O_3 appears to be due to insufficient reduction as indicated by the very small amount of CO uptake. As discussed under Introduction, many early workers (1–3) attributed the high activity of bimetallic Pt–Mo catalysts to Pt which was electronically modified by the presence of Mo. This notion has been changed, however, since the reactivity of well-reduced molybdenum catalysts was recognized. Fully reduced Mo catalysts are highly active in CO hydrogenation with turnover rates as high as those of Ru (26). Hence, in CO hydrogenation over bimetallic catalysts, the active site should be reduced Mo and the addition of Pt may have helped the reduction of molybdenum (22).

The conclusion that the active site of CO hydrogenation is reduced Mo with insignificant contribution from Pt sites makes CO chemisorption a less useful tool to count the number of catalytically active sites. CO chemisorption titrates both Mo and Pt nonselectively. Since the surface fraction of reduced molybdenum is unknown, TOF values represent weighted averages composed of low activity Pt sites and high activity Mo sites.

Temperature of reduction had a complicated influence on the bimetallic catalysts. EXAFS fitting showed similar structural parameters such as coordination number and interatomic distance for catalysts reduced at three temperatures. However, TOF values of CO hydrogenation show a substantial increase with the increase of reduction temperature. Furthermore, as the reaction progressed, the catalysts reduced at 1173 K lost its activity faster than those reduced at 773 and at 973 K. Both effects appear to have been due to a higher degree of reduction of active Mo sites in bimetallic catalysts reduced at a higher temperature. As indicated, as the reduction temperature increased, XANES of Mo K-edge (Fig. 4B) for the catalysts became more similar to that of Mo foil, indicating the existence of more metallic Mo phase.

CONCLUSIONS

XAFS demonstrated the formation of Pt–Mo alloy clusters on γ-alumina when the bimetallic catalysts were prepared by impregnation with respective metal salts. In the alloy clusters, molybdenum seemed to segregate to the surface and to adjust its metal–metal distance to that of platinum which resides near the core of the clusters. This structure did not depend on the sequence of metal addition onto the support. Almost all bimetallic $(Mo,Pt)/\gamma\text{-}Al_2O_3$ catalysts were much more active in CO hydrogenation than monometallic catalysts, $Pt/\gamma\text{-}Al_2O_3$ or $Mo/\gamma\text{-}Al_2O_3$. Reduced Mo appeared to be the active sites for the reaction and Pt seemed to help Mo sites become more reduced.

REFERENCES

1. Yermakov, Y. I., Kuznetsove, B. N., and Ryndin, Y. A., *J. Catal.* **42**, 73 (1976).
2. Tri, T. M., Candy, J.-P., Gallezot, P., Massardier, J., Primet, M., Vedrine, J. C., and Imelik, B., *J. Catal.* **79**, 396 (1983).
3. Tri, T. M., Massardier, J., Gallezot, P., and Imeik, B., *J. Catal.* **85**, 244 (1984).
4. Leclercq, G., Romero, T., Pietrzyk, S., Grimblot, J., and Leclercq, L., *J. Mol. Catal.* **25**, 67 (1984).
5. Rehr, J. J., Mustre de Leon, J., Zabinsky, S. I., and Albers, R. C., *J. Am. Chem. Soc.* **113**, 5135 (1991).
6. Bart, J. C. J., *Adv. Catal.* **34**, 203 (1986).
7. Matheiss, L. F., and Dietz, R. E., *Phy. Rev. B* **22**, 1663 (1980).
8. Sinfelt, J. H., "Bimetallic Catalysts: Discoveries, Concepts, and Applications." Wiley, New York, 1983.
9. Samant, M. G., Bergeret, G., Meitzner, G., and Boudart, M., *J. Phys. Chem.* **92**, 3542 (1988).
10. Samant, M., Bergeret, G., Meitzner, G., Gallezot, P., and Boudart, M., *J. Phys. Chem.* **92**, 3547 (1988).
11. Lee, J. S., Choi, S. H., Kim, K. D., and Nomura, M., *Appl. Catal. B* **7**, 199 (1996).
12. Teo, B.-K., "EXAFS: Basic Principles and Data Analysis." Springer-Verlag, Berlin, 1985.
13. Koningsberger, D. C., and Prins, R., (Eds.), "X-ray Absorption: Principles, Applications and Techniques of EXAFS, SEXAFS and XANES." Wiley, New York, 1988.
14. Lagarde, P., Murata, T., Vlaic, G., Freund, E., Dexpert, H., and Bournonville, J. P., *J. Catal.* **84**, 333 (1983).
15. Caballero, A., Villain, F., and Dexpert, H., *J. Chem. Soc. Faraday Trans.* **89**, 159 (1993).
16. Khanna, S. N., Bucher, J. P., and Buttet, J., *Surf. Sci.* **127**, 165 (1983).
17. Lee, J. S., Locatelli, S., Oyama, S. T., and Boudart, M., *J. Catal.* **125**, 157 (1990).
18. Lee, J. S., and Boudart, M., *Jpn. J. Appl. Phys.* **32**, 472 (1993).
19. Lee, J. S., and Boudart, M., *Catal. Lett.* **20**, 97 (1993).
20. Massoth, F. E., *Adv. Catal.* **27**, 265 (1978).
21. Zsoldos, Z., Hoffer, T., and Guczi, L., *J. Phys. Chem.* **95**, 798 (1991).
22. Guczi, L., Hoffer, T., Zsoldos, Z., Zyade, S., Maire, G., and Garin, F., *J. Phys. Chem.* **95**, 802 (1991).
23. Zsoldos, Z., and Guczi, L., *J. Phys. Chem.* **96**, 9393 (1992).
24. Toyoshima, I., and Somorjai, G. A., *Catal. Rev. Sci. Eng.* **19**, 105 (1979).
25. Vannice, M. A., *J. Catal.* **37**, 449 (1975).
26. Keller, C. S., and Bell, A. T., *J. Catal.* **75**, 251 (1981).
27. Saito, M., and Anderson, R. B., *J. Catal.* **63**, 438 (1980).
28. Lee, J. S., Yeom, M. H., and Lee, D.-S., *J. Mol. Catal.* **62**, L45 (1990).